Microstructure and ferromagnetic clusters in slightly doped $La_xBa_{4-x}Mn_3O_{10}$

L. D. Yao, W. Zhang, F. Y. Li, C. Q. Jin, and R. C. Yu[a)]
Laboratory for Extreme Condition Physics, Beijing National Laboratory for Condensed Matter Physics, Institute of Physics, Chinese Academy of Sciences, P.O. Box 603, Beijing 100190, People's Republic of China

(Received 25 September 2007; accepted 16 January 2008; published online 20 March 2008)

The nominal composition $La_xBa_{4-x}Mn_3O_{10}$ ($x=0-0.2$) compounds were synthesized using solid-state reaction under high pressure. The structures of the two single-phase samples $La_xBa_{4-x}Mn_3O_{10}$ ($x=0,0.05$) have been studied by powder x-ray diffraction, electron diffraction, and high-resolution transmission electron microscopy (HRTEM). For the $x=0.05$ sample, some intergrowth structures and stacking faults were revealed by HRTEM observations. According to the results of electron energy-loss spectroscopy (EELS) analysis, the slight doping of La into the parent phase compound $Ba_4Mn_3O_{10}$ was confirmed. Moreover, the L_3/L_2 intensity ratio of Mn-$L_{2,3}$ edges in the EELS spectra indicates the variation of Mn ionic valence state induced by the doping of La. Based on analysis of magnetic properties, the magnetization for the $x=0$ sample shows a broad peak centered around 170 K and a sharp upturn at low temperature of 15 K, which is due to a short-range low-dimensional antiferromagnetic ordering. For the $x=0.05$ sample, the slight doping of La leads to significant changes in magnetic properties. The zero-field cooled and field cooled magnetizations and hysteresis loop curves suggest that La doping induces ferromagnetic clusters in the antiferromagnetic matrix. © *2008 American Institute of Physics*. [DOI: 10.1063/1.2896587]

I. INTRODUCTION

Since the discovery of colossal magnetoresistance (CMR) effect[1,2] in manganese oxides with the perovskite structure $Ln_{1-x}A_xMnO_3$ (Ln is a rare-earth ion and A is an alkaline-earth cation), the extensive study interest has been focused on a series of manganese oxides $(Ln_{1-x},A_x)_{n+1}Mn_nO_{3n+1}$ with Ruddlesden–Popper (RP) structure and their magnetotransport properties.[3] The RP structure can be considered as an alternate stacking of n perovskite block layers and a rocksalt type layer. Thus, with changing the n, the number of MnO_2 sheets in these blocks varies, and the effective dimensionality can be adjusted. The network structure of Mn–O–Mn varies from full three-dimensional (3D) in the case of $n=\infty$, to two-dimensional (2D) or quasi-2D in the case of $n=1$, 2, or 3. The CMR effect and inherent anisotropic characteristics in charge transport and magnetic properties have been studied for the compounds with different values of n and doping level (x).

In the general formula $(Ln_{1-x},A_x)_{n+1}Mn_nO_{3n+1}$ compounds, different structures can be stabilized in the A–Mn–O (A-alkaline-earth) system as a function of the chemical nature of the A ion, the A/Mn ratio and the oxygen content. For $A=Ca$, a series of RP phases can be formed by conventional synthetic method, while in the case of $A=Sr$ and Ba, it is much more difficult to synthesize a RP phase. Remarkably, for the $n=3$ compounds, it was reported that $Ca_4Mn_3O_{10}$ compounds synthesized belong to the three-layered RP phase with an orthorhombic structure (space group *Pbca*) (Ref. 4) or a tetragonal structure (space group $I4/mmm$),[5] whereas $Sr_4Mn_3O_{10}$ and $Ba_4Mn_3O_{10}$ compounds[6,7] prepared possess another layered structure (space group *Cmca*) isotypic to $Cs_4Ni_3F_{10}$,[8] namely, the structure is built up from $[Mn_3O_{12}]$ units of three face-sharing octahedra, and two of these units are linked via their common apices through two of their three terminal corners to form zigzag sheets perpendicular to the b axis of the orthorhombic unit cell, and Sr (Ba) atoms occupy the space between the layers. Considering the structural difference between the RP phase for $Ca_4Mn_3O_{10}$ and the layered phases containing $[Mn_3O_{12}]$ trimers for $Sr_4Mn_3O_{10}$ and $Ba_4Mn_3O_{10}$, it is expected that their magnetic properties and magnetoresistance effect will show the obvious distinction. As for the former, there is weakened exchange couplings between the groups of layers as compared to the intralayer couplings, but the magnetic properties of the latter root in the compositive outcome of intratrimer and intertrimer interactions. In order to try to explore the influence of changing Mn ion valence on the magnetic properties and magnetoresistance behavior in the $n=3$ system, recently, a significant research effort has been fixed on the synthesis and characterization of the doping $(Ln_{1-x},A_x)_4Mn_3O_{10}$ compounds.[9–12] However, surprisingly it is very difficult to realize the substitution of Ln for A in the $n=3$ system, whether A is Ca or Sr and Ba. Even so, some groups reported that the slight doping compounds were synthesized successfully. For instance, we synthesized $La_xCa_{4-x}Mn_3O_{10}$ ($x=0,0.1$) compounds by means of solid-state reaction under high pressure and observed some intergrowth structures related to the perovskite blocks of $n=5$, 6, and 10 members.[13] Tang *et al.*[14] prepared slightly doped compounds $La_{3-3x}Sr_{1+3x}Mn_3O_{10}$ ($x=1.00,0.99,0.95$), and pointed out that slight electron doping leads to significant change in the magnetic properties due to the formation of ferromagnetic clusters. Up to now, although the magnetic and structural properties of polycrystalline $Ba_4Mn_3O_{10}$ have been studied carefully by neutron diffraction, specific heat, and magnetization measurements, little information on the microstructure and magnetic prop-

[a)]Author to whom correspondence should be addressed. Electronic mail: rcyu@aphy.iphy.ac.cn.

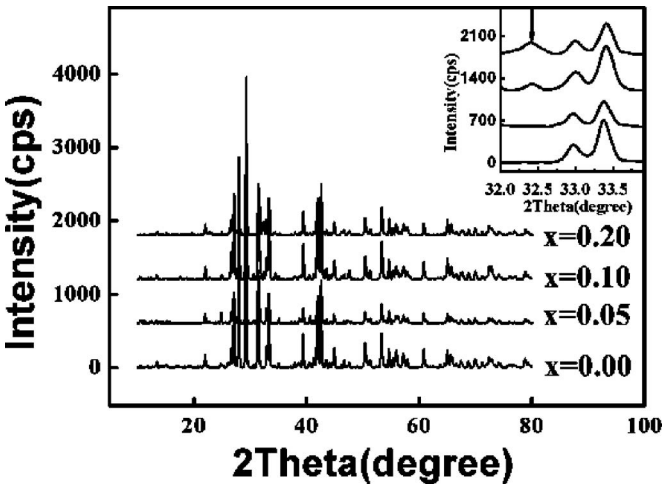

FIG. 1. Powder x-ray diffraction patterns of the $La_xBa_{4-x}Mn_3O_{10}$ ($x=0-0.2$) samples. The diffraction peak of an impurity phase is labeled by a black arrow in the inset.

erties of the doped compounds $Ln_xBa_{4-x}Mn_3O_{10}$ are available. In this paper, we report comparative results of structures and physical properties between $La_xBa_{4-x}Mn_3O_{10}$ ($x=0,0.05,0.1,0.2$).

II. EXPERIMENTS

Polycrystalline samples of nominal $La_xBa_{4-x}Mn_3O_{10}$ ($x=0,0.05,0.1,0.2$) were synthesized by using solid-state reaction under high pressure. Firstly, well-ground stoichiometric mixtures of $BaCO_3$, MnO_2, and La_2O_3 were pelletized and calcined in air at 900 °C for 12 h, and the resulting mixtures were reground, pelletized, and treated under the same conditions of 5.5 GPa and 1250 °C for 15 min. The detailed procedure of sample preparation was similar to that described elsewhere.[5]

The purities of the samples were checked by x-ray diffraction (XRD). The XRD patterns were collected with Rigaku rotating anode powder x-ray diffractometer (RINT 2000) operating with Cu $K\alpha_1$ radiation. Thin foils for transmission electron microscopy (TEM) studies were prepared by crushing the bulk specimen in an agate mortar filled with alcohol, and then dispersing the fine fragments suspended in alcohol on a microgrid. A Tecnai F20 field-emission electron microscope installed at Beijing Laboratory of Electron Microscopy, Beijing National Laboratory for Condensed Matter Physics, was used for electron diffraction (ED), high-resolution TEM (HRTEM), and electron energy-loss spectroscopy (EELS) experiments. All the TEM studies were carried out at an acceleration voltage of 200 kV. Magnetic properties were measured using a superconducting quantum interference device magnetometer.

III. RESULTS AND DISCUSSION

The XRD patterns of the $La_xBa_{4-x}Mn_3O_{10}$ ($x=0-0.2$) samples are shown in Fig. 1. For the $x=0$ sample, all the diffraction peaks can be indexed according to an orthorhombic structure with a space group of *Cmca*, in consistent with the results in Ref. 7. With the slight doping of La ($x<0.05$), no diffraction peaks of impurity phase are observed,

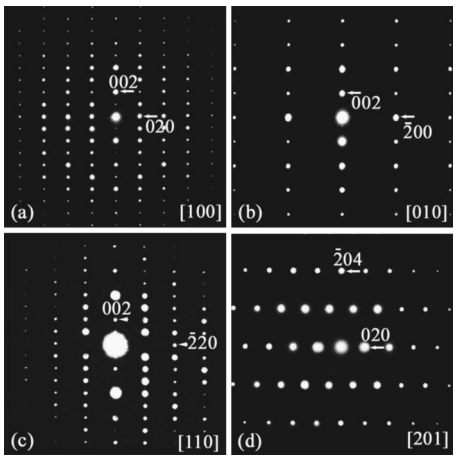

FIG. 2. ED patterns taken along different zone axes for the $La_xBa_{4-x}Mn_3O_{10}$ ($x=0.05$) sample. (a) [100], (b) [010], (c) [110], and (d) [201].

in contrast with that of the $x=0$ sample, which confirms that the $x=0.05$ sample belongs to a single phase. However, diffraction peaks of impurity phase, as is denoted by arrow in inset of Fig. 1, gradually show up with the increase of La doping level over 0.05. According to the analyses of all patterns, a single-phase sample is difficult to be formed by substituting barium with lanthanum for high doping level. In this paper, the $x=0$ and 0.05 samples are mainly discussed since they are single-phase compounds.

ED patterns were obtained from the $x=0$ and 0.05 samples. Figure 2 shows a series of selected area ED patterns from different zone-axis directions for the $x=0$ sample. Based on these ED patterns, the reciprocal space of the compound has been reconstructed and can be indexed with a *C* centered orthorhombic lattice. The systematic extinction conditions are observed to be *hkl*: $h+k=2n$; *hk*0: $h=2n$; and *h*0*l*: $h+l=2n$. Here, it should be noted that the appearance of 00*l* ($l=2n+1$) reflections in Fig. 2(a) are due to the double diffraction in the thicker crystal zone. According to the above extinction rules, the space group *Cmca* can be uniquely determined. The lattice parameters were derived from the ED patterns as $a\approx0.56$ nm, $b\approx1.31$ nm, and $c\approx1.27$ nm, which is close to the results of XRD analysis. Due to the same crystal structure, the $x=0$ and 0.05 samples have same diffraction pattern features.

Figure 3(a) shows a HRTEM image obtained from [100] zone-axis direction for the $x=0.05$ sample, indicating an ap-

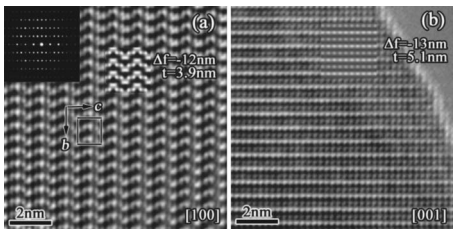

FIG. 3. (a) HRTEM image of the $x=0.05$ sample taken along the [100] zone-axis direction. The corresponding ED pattern taken along the [100] direction is shown on the top left-hand corner of the image. One unit cell is outlined using black solid lines, and a simulated image is superimposed onto the experimental image. (b) HRTEM image of the $x=0.05$ sample taken along the [001] zone-axis direction. A simulated image is superimposed onto the experimental image.

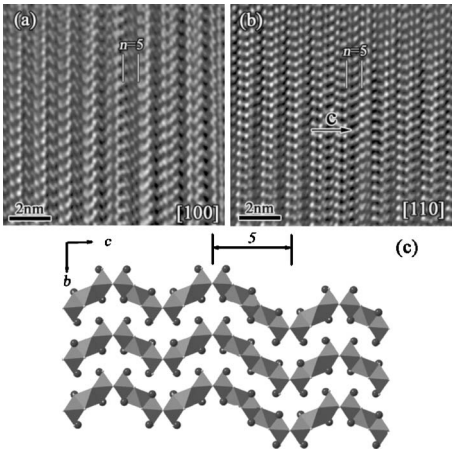

FIG. 4. (a) [100] and (b) [110] zone-axis HRTEM images of the area containing an intergrowth block of $n=5$ member, respectively. (c) Schematic [100] projection of the $n=3$ $Ba_4Mn_3O_{10}$ structure containing an intergrowth block of $n=5$ member.

parently well ordered material with d spacings 6.5 and 12.7 Å, where the contrast forms clearly a zigzag path along c axis. The corresponding ED pattern is shown on the top left-hand corner of Fig. 3(a) and also indicates the details of the layered structure. Moreover, black solid lines outline one unit cell. In Fig. 3(b), a HRTEM image taken along [001] zone axis is also shown. Image simulations based on the structure model proposed previously[7] were carried out on the simulation program JEMS using multislice theory of dynamical scattering. The simulated results show that the simulated images for the two different zone axes, superimposed onto the images, appear to be in good agreement with the experimental ones. Interestingly, although the $x=0.05$ sample shows a single phase with layered $Ba_4Mn_3O_{10}$ structure from the XRD data, the presence of some structural defects in some microzones, especially intergrowth faults of the hexagonal $Ba_{n+1}Mn_nO_{3n+1}$ homologous series, is revealed by TEM. Similar to the results observed by Yang *et al.*[15] recently in $Ba_6Mn_5O_{16}$ compound, intergrowth structures are also easily formed in our sample, which can be characterized by HRTEM along both the [100] and [110] zone-axis directions. As examples, Fig. 4(a) shows the [100] zone-axis HRTEM image of an area containing $n=5$ member hexagonal structure and Fig. 4(b) presents the [110] zone-axis HRTEM image including the same intergrowth structure from another microzone. In order to well understand the formation of the intergrowth faults, we show schematically in Fig. 4(c) the [100] projection of the $n=3$ $Ba_4Mn_3O_{10}$ structure containing the $n=5$ block, where it can been seen that the intergrowth block is generated by the substitution of a group of $[Mn_5O_{18}]$ units with five face-sharing octahedra for a group of $[Mn_3O_{12}]$ units with three face-sharing octahedra.

Besides the intergrowth structure, occasionally in some microzones, the stacking faults were also observed and the corresponding HRTEM image is shown in Fig. 5(a). The formation of this kind of faults can be understood as the fact that one part of single crystal grain glides relative to the other part occurring on a certain plane of O atoms (bridging the neighboring $[Mn_3O_{12}]$ units by vertex-sharing style) along $\boldsymbol{b}$ zone-axis direction, and slip vector is $\boldsymbol{b}/4$. In order

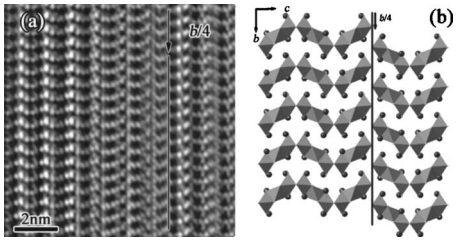

FIG. 5. (a) [100] zone-axis HRTEM images of an area containing a stacking fault. (b) Schematic [100] projection of the $n=3$ $Ba_4Mn_3O_{10}$ structure containing the stacking faults.

to clearly illustrate the formation, the [100] projection of the $n=3$ $Ba_4Mn_3O_{10}$ structure including this fault is shown schematically in Fig. 5(b). Obviously, structure distortion would occur near the slip plane due to the misfit of lattice, and it is possible that the absence of oxygen is accompanied. Moreover, it should be noticed that some strong white dots are observed in the left side part and not in the middle part in Fig. 5(a). This feature can be viewed as the results from the inhomogeneous distributions of La and Ba ions.

In order to further confirm the two compounds from a chemical point of view, EELS studies were also carried out. Figure 6(a) shows the EELS spectra including Ba-$M_{4,5}$ absorption edges obtained from $x=0$ and 0.05 samples along [100] zone-axis direction. It is clear that La-$M_{4,5}$ absorption edges appear at about 832 eV for the $x=0.05$ sample in Fig. 6(b), which confirms the slight doping of La into the parent compound $Ba_4Mn_3O_{10}$. On the other hand, EELS can also supply direct evidence of variation of Mn ionic valence state, since Mn ionic valence falls due to the addition of La content. Figure 6 shows the EELS spectra including Mn-$L_{2,3}$ absorption edges obtained from the $x=0$ and 0.05 samples along [100] zone-axis direction. We normalized the two spectra in Fig. 6 to have the same Mn-L_3 edge integrated counts. By comparing the Mn-$L_{2,3}$ edges, one can see that the L_3/L_2 intensity ratio rises with the doping of La ions, indicating that Mn ions in the $x=0.05$ sample show up a lower valence state according to the well known relationship between the L_3/L_2 intensity ratio and the valence state for Mn ions.[16]

Figure 7 shows the temperature dependence of the zero-field-cooled (ZFC) and field-cooled (FC) susceptibility in 0.1 T for $x=0$ and 0.05 samples. For the $x=0$ sample, the susceptibility curve $\chi(T)$ shows a broad peak centered at about 170 K and a sharp rise at low temperature of 15 K. The broad peak in $\chi(T)$ is a characteristic of low-dimensional antiferromagnetically coupled spin systems, while the rise at low temperatures is rather unusual. So it suggests that this is not a transition from a high temperature paramagnetic state to a low temperature 3D antiferromagnetic (AFM) state. As is well known, the zigzag $[Mn_3O_{12}]$ trimers extend along z-axis direction in $Ba_4Mn_3O_{10}$. Moreover, it has been reported that all Mn–Mn interactions are inherently AFM, and the magnetic properties of this kind of compound are the resultant of intratrimer and intertrimer interactions. Considering that there is low dimensional AFM structure in this material, we fit our susceptibility curve $\chi(T)$ with an expression of the following form:

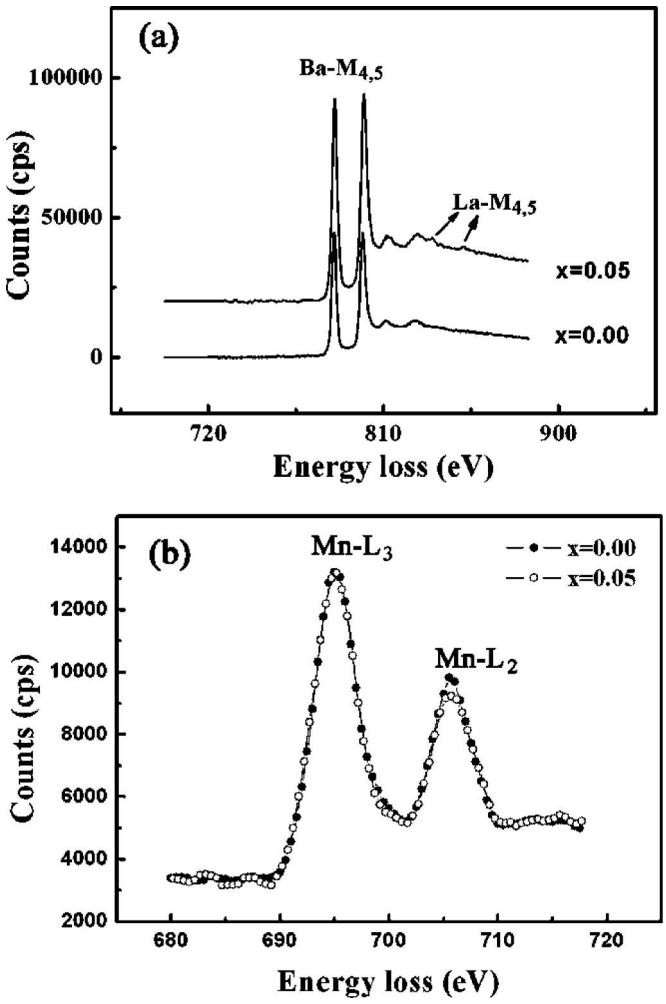

FIG. 6. (a) EELS spectra obtained from the $x=0$ and 0.05 samples along the [100] zone-axis direction. (b) Normalized EELS spectra including Mn-$L_{2,3}$ edges obtained from the doped and undoped samples along the [100] zone-axis direction.

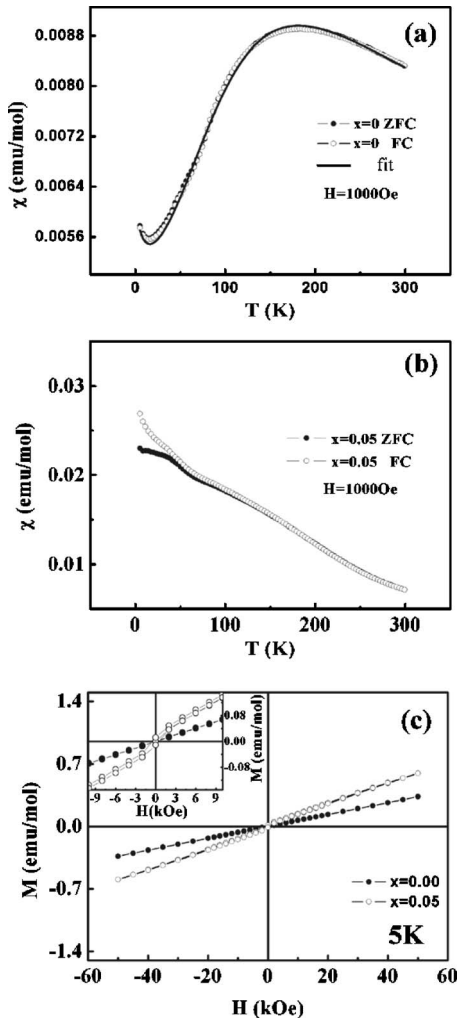

FIG. 7. (a) FC and ZFC magnetic susceptibility curves for the $x=0$ sample. The solid line is the fit of χ (T) using Eq. (1). (b) FC and ZFC magnetic susceptibility curves for the $x=0$ sample. (c) Hysteresis loops obtained at 5 K after cooling in a zero magnetic field for the $La_xBa_{4-x}Mn_3O_{10}$ ($x=0, 0.05$) samples. The inset on the top right corner shows an enlarged view of the hysteresis loops.

$$\chi(T) = \chi_{1D}(T) + \chi_{LT}(T) + \chi_{VV}(T). \quad (1)$$

$\chi_{1D}(T)$ is the Bonner–Fisher susceptibility of a one-dimensional (1D) AFM spin chain.[17,18] We took the polynomial approximation of Feyerherm[19] (valid for $T > 0.05$ J/kB).

$$\chi_{1D}(T) = \frac{N_A \mu_{eff}^2}{3k_B T} \frac{1 + 0.154\,65x + 0.273\,95x^2}{1 + 1.148\,64x + 0.946\,27x^2 + 8.566\,42x^3}, \quad (2)$$

where $x = |J|/k_B T$. The rise at low temperature was accounted for by Curie–Weiss term $\chi_{LT}(T)$,

$$\chi_{LT}(T) = \frac{C}{T + \theta}, \quad (3)$$

where $\chi_{VV}(T)$ is a temperature-independent Van-Vleck susceptibility.

Following the above approach, the experimental data can be fitted with Eq. (1) in the temperature range of 5 K $< T <$ 300 K. As shown in Fig. 7(a), the fit is shown as solid line with parameters $\mu_{eff} = 3.9\mu_B$ and $J = 78$ K. Although the μ_{eff} value is close to the theoretical effective moment of the Mn^{4+} free ion ($3.87\mu_B$), the experimental data cannot be fitted perfectly by Eq. (1), which suggests $Ba_4Mn_3O_{10}$ does not belong to 1D AFM spin system, but quasi-1D or 2D AFM spin system. However, the fit does support the picture of low dimensional antiferromagnetically coupled spin system for the $x=0$ sample. Here, it should be pointed out that the magnetic behavior of the $x=0$ sample at lower temperatures is very different from the previous report for the $Ba_4Mn_3O_{10}$.[7] In our sample, the sharp but limited rise for magnetic susceptibility is shown at about 15 K, less than 40 K previously reported for $Ba_4Mn_3O_{10}$. This is probably resulted from the difference of oxygen content since our sample was prepared by high-pressure method.

For the $x=0.05$ sample, the magnetization curve, shown in Fig. 7(b), is quite different from that of the $x=0$ sample. The shape of the curve shows a weak ferromagnetismlike behavior. Moreover, it is also seen that the FC and ZFC data diverge below 50 K, which indicates that either inhomogeneous clusters or homogeneous spin-glass phase is induced by La doping at low temperature.[14] In principle, the small

ferromagnetic component of the magnetization in the ordered state could have two distinct explanations. One is that the double exchange (DE) interaction appears. For instance, in the hole-doped CMR manganites, where the mixed valence of Mn^{3+} and Mn^{4+} occurs, the ferromagnetism is explained within the framework of the DE, i.e., the mobile e_g electron supplied by the Mn^{3+} ions ferromagnetically couple the localized t_{2g} spins of a Mn^{3+}–Mn^{4+} neighboring pair. The other is the existence of Dzyaloshinski–Moriya term[20,21] introduced by the orthorhombic distortion of the crystal structure. As an example, in the $Ca_4Mn_3O_{10}$ compound Lago *et al.*[4] reported that the weak ferromagnetic component is mainly attributed to the latter. Clearly, for our $x=0.05$ sample, due to the slight doping of La, the magnetic increases with the existence of the Mn^{3+} ions. The DE origin of the weak ferromagnetic component is mainly considered in view of a small concentration of e_g electrons on the Mn^{4+} lattice. In addition, although some structure faults in some microzones were revealed by HRTEM for the $x=0.05$ sample, they can play a positive role in the DE coupling. In the intergrowth structures, La doping can also enhance the appearance of Mn^{3+} ions in $n=3$ blocks, thus, the stronger intramultimer (Mn_5O_{18}) interactions contribute to the short-range ferromagnetic (FM) clusters. At the same time, the deficiency of oxygen near the stacking faults can induce the decrease of the valence of Mn ions, the similar positive effect exists, which favors the DE coupling. Thus, it is concluded that FM clusters often appear easily in some microzones, especially with the intergrowths or stacking faults.

To further study the magnetic structure of the samples, we also measured M versus H curves at 5 K, as plotted in Fig. 7(c). The hysteresis loops for the $x=0$ sample at 5 K show a linear field dependence of the magnetization arising from the AFM framework. For the $x=0.05$ sample, magnetization rises sharply with the increase of field. As is shown in the inset of Fig. 7(c), the hysteresis is observed at $H<1500$ Oe and the magnetization does not saturate even at 50 kOe. Taking into account the fact that the hysteresis appears at a high field for spin glass, it is more likely that the La doping results in FM clusters rather than a spin-glass state, and the FM clusters are embedded in an AFM matrix, which is similar to the results of Tang *et al.*[14] in $La_xSr_{4-x}Mn_3O_{10}$ compounds.

IV. CONCLUSIONS

In our experiments, the nominal composition $Ba_{4-x}Mn_3O_{10}$ ($x=0-0.2$) compounds were prepared by means of high-pressure method. Through the results of XRD and ED analyses, $Ba_{4-x}Mn_3O_{10}$ ($x=0$ and 0.05) compounds belong to a single-phase orthorhombic structure with a space group of *Cmca*, which is in good agreement with the corresponding report. For the $x=0.05$ sample, the presence of some structural defects in some microzones, especially $n=5$ intergrowth block in the $n=3$ parent structure, were revealed by HRTEM. Moreover, the stacking faults were also observed in one part of crystal glides relative to the other part on a certain plane of O atoms (bridging the neighboring $[Mn_3O_{12}]$ units by vertex-sharing style) along $\boldsymbol{b}$ zone-axis direction, and slip vector is $\boldsymbol{b}/4$. According to the results of EELS analysis, La-$M_{4,5}$ absorption edges appear at about 832 eV for the $x=0.05$ sample confirming the slight doping of La into the parent compound $Ba_4Mn_3O_{10}$. At the same time, by comparing L_3/L_2 intensity ratio of the Mn-$L_{2,3}$ edges between doped and undoped samples, it is indicated that Mn ions in the $x=0.05$ sample show up a lower valence state due to the doping of La ions. For the $x=0$ sample, the magnetic susceptibility curve shows a characteristic of a low dimensional antiferromagnetically coupled spin systems. For the La doped samples, Mn^{3+} ions are created from Mn^{4+}, thus, the DE coupling between Mn^{3+} and Mn^{4+} leads to FM clusters around Mn^{3+} sites. Moreover, the deficiency of oxygen near the stacking faults and the La doping in the intergrowth structures can contribute to decreasing the valence of Mn ions, further play a positive role in the DE interaction. Because of the little amounts of La and the anisotropic coupling, the doped electrons appear to remain essentially localized. As a result, there is no long range FM ordering but the presence of FM clusters embedded in an AFM matrix.

ACKNOWLEDGMENTS

This work was supported by the National Natural Science Foundation of China (Grant Nos. 10774168, 50471053, and 50621061) and the State Key Development Program for Basic Research of China (Grant Nos. 2005CB623602 and 2007CB925003).

[1] R. M. Kusters, J. Singleton, D. A. Keen, R. Mcgreevy, and W. Hayes, Physica B **155**, 362 (1989).
[2] R. von Helmolt, J. Wecker, B. Holzapfel, L. Schultz, and K. Samwer, Phys. Rev. Lett. **71**, 2331 (1993).
[3] Y. Moritomo, A. Asamitsu, H. Kuwahara, and Y. Tokura, Nature (London) **380**, 141 (1996).
[4] J. Lago, P. D. Battle, and M. J. Rosseinsky, J. Phys.: Condens. Matter **12**, 2505 (2000).
[5] R. C. Yu, S. Y. Li, J. L. Zhu, F. Y. Li, Z. Zang, C. Q. Jin, and I. G. Voigt-Martin, J. Appl. Phys. **90**, 6302 (2001).
[6] N. Floros, M. Hervieu, G. V. Tendeloo, C. Michel, A. Maignan, and B. Raveau, Solid State Sci. **2**, 1 (2000).
[7] V. G. Zubkov, A. P. Tyutyunnik, I. F. Berger, V. I. Voronin, G. V. Bazuev, C. A. Moore, and P. D. Battle, J. Solid State Chem. **167**, 453 (2002).
[8] R. Schmidt, J. Pebler, and D. Babel, Eur. J. Solid State Inorg. Chem. **29**, 679 (1992).
[9] H. J. Rossell, P. Goodman, S. Bulcock, R. H. March, S. J. Kennedy, T. J. White, F. J. Lincoln, and K. S. Murray, Aust. J. Chem. **49**, 205 (1996).
[10] N. S. Witte, P. Goodman, F. J. Lincoln, R. H. March, and S. J. Kennedy, Appl. Phys. Lett. **72**, 853 (1998).
[11] H. Asano, J. Hayakawa, and M. Matsui, Appl. Phys. Lett. **71**, 844 (1997).
[12] P. M. Sousa, M. D. Carvalho, M. E. Melo Jorge, F. M. Costa, M. M. Cruz, and M. Godinho, Solid State Sci. **5**, 943 (2003).
[13] L. D. Yao, H. Yang, W. Zhang, F. Y. Li, C. Q. Jin, and R. C. Yu, J. Appl. Phys. **100**, 023907 (2006).
[14] Y. K. Tang, X. Ma, Z. Q. Kou, Y. Sun, N. L. Di, Z. H. Cheng, and Q. A. Li, Phys. Rev. B **72**, 132403 (2005).
[15] H. Yang, R. F. Yang, Q. A. Li, F. Y. Li, C. Q. Jin, and R. C. Yu, J. Phys. Chem. Solids **67**, 2365 (2006).
[16] Z. L. Wang, J. S. Yin, and Y. D. Jiang, Micron **31**, 571 (2000).
[17] J. C. Bonner and M. E. Fisher, Phys. Rev. **135**, A640 (1964).
[18] W. E. Hatfield, J. Appl. Phys. **52**, 1985 (1981).
[19] R. Feyerherm, S. Abens, D. Günther, T. Ishida, M. Meißner, M. Meschke, T. Nogami, and M. Steiner, J. Phys.: Condens. Matter **12**, 8495 (2000).
[20] I. Dzyaloshinskii, J. Phys. Chem. Solids **4**, 241 (1958).
[21] T. Moriya, Phys. Rev. **120**, 91 (1960).